Tellus (2002), 54A, 14–33
Printed in UK. All rights reserved

TELLUS
ISSN 0280–6495

Structure function characteristics for 2 metre temperature and relative humidity in different horizontal resolutions

By KAI SATTLER* and XIANG-YU HUANG, *Danish Meteorological Institute, Lyngbyvej 100, DK-2100 Copenhagen Ø, Denmark*

(Manuscript received 19 January 2001; in final form 27 August 2001)

ABSTRACT

The isotropic correlations of forecast errors in the HIRLAM system are investigated for different horizontal grid sizes in order to achieve an improved representation of the structure functions for high-resolution surface analysis. The investigation is performed for 2 metre temperature and relative humidity and makes use of operational forecasts from DMI-HIRLAM at the Danish Meteorological Institute (DMI), which can support the background for a surface analysis in three different horizontal resolutions. Two different well-known methods for determining isotropic forecast error correlations are applied. The first method compares forecasts to observations (the Observation Method), while the second makes use of two different forecasts valid for the same time (the NMC Method). The latter method is also used to investigate isotropy as well as the influence of land–sea contrast and orography. A comparison of the two mentioned methods reveals a good correspondence between them, and the investigation of monthly changes shows some seasonal tendencies. The isotropy assumption is shown to be acceptable to a first approximation, despite a slight dependency on the predominant flow. The results further suggest a decrease in the background error correlation scales when going to higher horizontal resolution in the forecast model.

1. Introduction

During recent years, the trend towards high-resolution weather forecasting has continued. Connected to this has been the development of analysis schemes for temperature, humidity, wind and other parameters at near-surface levels (Navascues, 1997) as well as in the mesoscale (Häggmark et al., 2000). These schemes are based on optimum interpolation (OI) (Gandin, 1963) and, apart from the fact that they are univariate and two-dimensional (horizontal), are similar to the analysis schemes that have been used for upper level parameters in many operational numerical weather prediction systems (Lorenc, 1981; Daley, 1996).

* Corresponding author.
e-mail: ksa@dmi.dk

Within the calculation of the analysis increment, the statistical structure functions play a major role. This is equally valid for OI type schemes and for three-dimensional variational (3DVAR) type schemes (Lorenc, 1986). In univariate schemes, each function represents the spatial background error correlations of a certain variable (Hollingsworth and Lönnberg, 1986). These correlations are often assumed to be isotropic and homogeneous in order to simplify the analysis (Daley, 1991). One way to estimate the background error correlations is to use both background and observations, as proposed by Rutherford (1972), Hollingworth and Lönnberg (1986) and Lönnberg and Hollingworth (1986). The method has been used for years and will be referred to as the Observation Method. The determination of the structure functions by this method necessitates a reliable and homogeneous

observation network. An alternative to the Observation Method is the exclusive use of forecast data when evaluating the structure functions (Parrish and Derber, 1992). The method is often referred to as the NMC Method and has been successfully applied in recent years (e.g. Parrish and Derber, 1992; Rabier et al., 1998; Derber and Buttier, 1999; Berre, 2000; Gustafsson et al., 2001; Ingleby, 2001; Lorenc et al., 2000). Since both methods require a homogeneous series of forecasts, the structure functions need to be re-evaluated as soon as the forecast model is changed at some major points (Puri and Lönnberg, 1991). Yet another possibility is to make use of a Kalman filter when evaluating forecast error correlations. The method is described by Bouttier (1994) and makes a dynamical evaluation possible, contrary to the above-mentioned approaches.

A scheme for the analysis of 2 metre temperature (T2m) and relative humidity (RH2m) was developed within the international HIRLAM cooperation (Navascues, 1997). The structure functions used in the analysis scheme take care of land–sea contrast (Gustafsson, 1985) and changes in surface elevation (Navascues, 1997). This so-called surface analysis scheme of HIRLAM is applied at the Spanish weather service INM (Garçia-Moya et al., 2000) and was recently applied at the Danish Meteorological Institute DMI (Sattler et al., 2000).

In the study of Sattler et al. (2000), in which the surface analysis for T2m and RH2m was applied over Denmark in a very high horizontal grid spacing of 5 km, the quality of the analysis was found to be unsatisfactory. The authors suspected the scales of the structure functions for T2m and RH2m to be inadequate for this grid spacing and proposed a re-evaluation, leading to the motivation of this study.

The Observation Method, the NMC Method and some considerations for their application are described in Section 2. The major results are presented in Section 3. Some conclusions are drawn in Section 4 and a list of symbols is included in the Appendix.

2. Structure function determination

2.1. Observation Method

The Observation Method determines a distance-dependent structure function for the correlation of the difference between background and observation by building correlations between all available observation locations. The relation between the grid points of the forecast model and the observation locations can be described by the linear observation operator $\boldsymbol{H}$:

$$\boldsymbol{y}^{\mathrm{t}} = \boldsymbol{H}\boldsymbol{x}^{\mathrm{t}}. \tag{1}$$

Refer to the list of symbols for a description of the variables. The background data usually refer to 6 h forecasts and is determined at the observation locations:

$$\boldsymbol{y}^{\mathrm{b6}} = \boldsymbol{H}\boldsymbol{x}^{\mathrm{b6}}. \tag{2}$$

$\boldsymbol{H}$ is realized by interpolation in this work. The error covariance between two points i and j is then defined as

$$b_{ij}^{6h} = \langle (y_i^{\mathrm{b6}} - y_i^t)(y_j^{\mathrm{b6}} - y_j^t) \rangle, \tag{3}$$

where the pointed brackets denote the expectation value. The observation error covariance is analogously defined as

$$r_{ij} = \langle (y_i^{\mathrm{o}} - y_i^t)(y_j^{\mathrm{o}} - y_j^t) \rangle. \tag{4}$$

If we assume that there is no correlation between observation errors and background errors when regarding two arbitrarily chosen points, then the sum of eqs. (3) and (4) leads to

$$s_{ij} = b_{ij}^{6h} + r_{ij} = \langle (y_i^{\mathrm{b6}} - y_i^{\mathrm{o}})(y_j^{\mathrm{b6}} - y_j^{\mathrm{o}}) \rangle. \tag{5}$$

The sum of the covariances can be determined from available observation data and the respective model fields without knowing the true values y^{t}. By introducing a normalization using the autocorrelations as proposed by Daley (1991), we can determine a correlation of differences between background and observation for the two locations i and j:

$$\mathrm{Corr}^{\mathrm{bo}}(i,j) = \frac{b_{ij}^{6h} + r_{ij}}{(s_{ii}s_{jj})^{1/2}}. \tag{6}$$

If we further assume that the observations at different sites are not correlated, then

$$r_{ij} = 0 \quad \text{for } i \neq j, \tag{7}$$

and (6) reduces to

$$\mathrm{Corr}^{\mathrm{bo}}(i,j) = \frac{b_{ij}^{6h}}{(s_{ii}s_{jj})^{1/2}} \quad \text{for } i \neq j. \tag{8}$$

The correlation determined in this way still contains an uncertainty, which is due to a possible bias in the background fields. In order to reduce the influence of this bias, the following correction

is applied for the whole area to the interpolated data:

$$y^{b6}_{biascor} = y^{b6} = \langle y^{b6} - y^{o} \rangle. \quad (9)$$

2.2. NMC Method

Errors which occur within the forecast model propagate with a certain speed within the model domain. Thus, variables at a certain grid point become first influenced by errors from distant grid points after a certain amount of time. As a result, the correlation of two forecast fields, which are valid at the same time, but which refer to different forecast lengths, must include information about the state of propagation of such errors. The correlation of two such forecasts originating from the same model shows a spatial structure. This structure is similar to the correlations found with the Observation Method, and may be used to find error correlation scales (Parrish and Derber, 1992). It can be regarded as isotropic to a first approximation.

The formulation for calculating the correlations is analogous to the Observation Method, but does not use observation data. The assumption of the Observation Method that there is no correlation between observation errors and background errors is not required by the NMC Method.

Within this work, 36 h forecasts and 12 h forecasts started 24 h later are used. The forecast error covariances for these two forecast lengths are defined analogously to eq. (3).

If we now assume that the covariance of the forecast differences between two model grid points m and n is proportional to the background error covariance, i.e.

$$\langle (x^{f12}_m - x^{f36}_m)(x^{f12}_n - x^{f36}_n) \rangle = \alpha b^{6h}_{mn}, \quad (10)$$

then the use of 12 h and 36 h forecasts will reveal similar covariance functions to using observations and 6 h forecasts.

With the introduction of a normalization as in the Observation Method by using the autocorrelations, we finally get for the correlation from the NMC Method:

$$\mathrm{Corr}^{ff}(m, n) = \frac{\langle (x^{f12}_m - x^{f36}_m)(x^{f12}_n - x^{f36}_n) \rangle}{[\langle (x^{f12}_m - x^{f36}_m)^2 \rangle \langle (x^{f12}_n - x^{f36}_n)^2 \rangle]^{1/2}}.$$

A correction due to forecast bias is not considered here, because both fields originate from the same forecast model.

2.3. Quality control

When applying the Observation Method, the results can be blurred when erroneous observations occur. It is therefore necessary to introduce a quality check in order to reject such data. With the simple assumption that the difference between background and observation must not exceed a given limit, we formulate

$$|y^{b6} - y^{o}| < \Delta y_{max}, \quad (12)$$

which at least ensures that gross errors are excluded.

2.4. Consistency

The correlation functions determined with the two above-mentioned methods and described by eqs. (8) and (11), respectively, contain a significant difference as distance approaches to zero. While

$$\lim_{d \to 0} \mathrm{Corr}^{ff} = 1 \quad (13)$$

for the function from the NMC Method, eq. (11), the limit for the function from the Observation Method, eq. (8), is

$$\lim_{d \to 0} \mathrm{Corr}^{bo} = \frac{(\sigma_b)^2}{(\sigma_b)^2 + (\sigma_o)^2}, \quad (14)$$

because the observation errors are assumed to be spatially uncorrelated, so only the local errors contribute to the correlation (Daley, 1991). This means that the correlation curve determined with the Observation Method only includes correlations that are due to the background error.

In order to compare the structure functions determined with the two methods, a further normalization of Corr^{bo} is necessary. It is possible to normalize Corr^{bo} by using the limit from eq. (14), so that $\mathrm{Corr}^{bo} \to 1$ as $d \to 0$. However, this limit is not really known, because σ_o is unknown. It includes the random observation error, an instrument error and the uncertainty of representativeness of the observation. A quite useful estimation of the limit is possible though, if Corr^{bo} is fitted to a representative function near $d = 0$. The intersection at $d = 0$ then is a good approximation for the limit of eq. (14).

It is assumed that the correlation curves behave

in a way in which the first deviation with respect to d is steady and goes to zero at $d = 0$. A suitable function to fit the curves for small values of d is a Gaussian function:

$$\mathrm{Corr}^{\mathrm{bo}}(d) = \mathrm{Corr}^{\mathrm{bo}}(0) \exp\left(-\frac{d^2}{2D^2}\right) \tag{15}$$

for $0 \leqslant \leqslant d_{\mathrm{fit}}$.

Even though this kind of function cannot be regarded as a suitable correlation model for the whole distance range (Julian and Thiebaux, 1975), it mainly differs from the generally used correlation models (Daley, 1991; Häggmark et al., 2000) in the tail of the function, rather than close to the origin.

The limit d_{fit} should be chosen such that it is large enough to cover the first points of $\mathrm{Corr}^{\mathrm{bo}}$ that are represented in the respective model. The value of $\mathrm{Corr}^{\mathrm{bo}}(0)$ and D are determined during the fitting process. This further normalization of $\mathrm{Corr}^{\mathrm{bo}}$ is then:

$$\mathrm{Corr}^{\mathrm{bos}}(d) = \frac{\mathrm{Corr}^{\mathrm{bo}}(d)}{\mathrm{Corr}^{\mathrm{bo}}(0)}. \tag{16}$$

$\mathrm{Corr}^{\mathrm{bos}}$ is consistent with $\mathrm{Corr}^{\mathrm{ff}}$ and makes direct comparison possible.

3. Structure functions in DMI-HIRLAM

3.1. General

The following investigations are performed using data from the operational NWP Model HIRLAM at DMI, DMI-HIRLAM-G, DMI-HIRLAM-E and DMI-HIRLAM-D (Sass et al., 1999). The investigations are divided into several parts. In the first part, the purpose is to find appropriate limits for the quality check in the application of the Observation Method. We show the isotropic properties of the forecast error correlations of DMI-HIRLAM in the second part by looking at the horizontal correlation fields, making use of the NMC Method. This also points to a dependency of correlation from the land–sea distribution. The other parts are then concerned with the investigation of the isotropic forecast error correlations in DMI-HIRLAM.

The structure function evaluations are performed with data from the three operational models DMI-HIRLAM-G, DMI-HIRLAM-E and DMI-HIRLAM-D. The three models are described on a rotated geographical grid with a horizontal grid spacing of 0.45°, 0.15° and 0.05°, respectively. The vertical is described by 31 levels in all three models, with the lowest level referring to approximately 30 m above ground level. The model domains are shown in Fig. 1. The significant difference of their size may cause some uncertainties when comparing structure functions. However, it can be assumed that the forecast errors of 2 metre temperature and relative humidity are mainly influenced by changes of the surface properties like land–sea contrast, which has been taken into account by the models (see below). Where the selection of observations is concerned, an equivalent set of observation sites is chosen for DMI-HIRLAM-G and DMI-HIRLAM-E. It contains 288 synoptic stations. The set used for DMI-HIRLAM-D includes a subset of 200 sites from these stations.

The Observation Method is applied as follows. Forecast fields based on analysis at 00 UTC and 12 UTC and valid 6 h later are compared to synoptic observations from 06 UTC and 18 UTC, respectively. The correlations of the differences are then referred to the distance between the respective sites. In addition to the quality control mentioned in Section 2.3, a control of sample size is applied to reject those samples which have sample size below 10 per month, before the correlation determination.

The NMC Method is applied to the 12 h

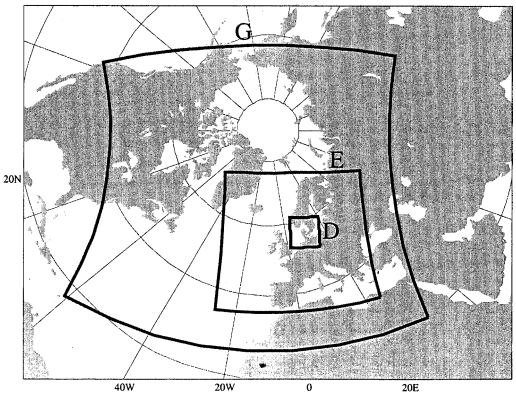

Fig. 1. Areas covered by the three operational models DMI-HIRLAM-G, DMI-HIRLAM-E and DMI-HIRLAM-D. The grid representation is in rotated geographic coordinates.

forecast based on 00 UTC analysis and the respective 36 h forecast from the day before. The correlations are determined for selected pairs of grid points and referred to the respective geographic distance between them.

The calculated correlations are not shown, but empirically averaged correlations for the selected separation intervals (Hollingsworth and Lönnberg, 1986). As the correlation samples are large and include at least several hundred elements per averaging interval, arithmetic averaging seems appropriate.

3.2. *Quality control limits*

As outlined in Section 2.3, a quality check of the observations is applied, but the quality control limit $\Delta y_{\max}$ is still to be determined.

The limits for rejecting observation data are determined for both 2 metre temperature (T2m) and relative humidity (RH2m). Data from January and February 2000 are examined using the bias correction (9). We assume that the results are generally valid. Figure 2 shows correlation curves for the low resolution model DMI-HIRLAM-G. The effect from applying different limits in the quality control can be clearly recognized for both months. The same is valid for DMI-HIRLAM-E (not shown) and DMI-HIRLAM-D (Fig. 3).

The correlation in T2m drops remarkably for those differences which are below 5 K. For RH2m, this limit is 30%. This indicates that the small errors tend to behave more randomly than the larger errors. The curve referring to a limit of 2 K for T2m from February still shows some bias,

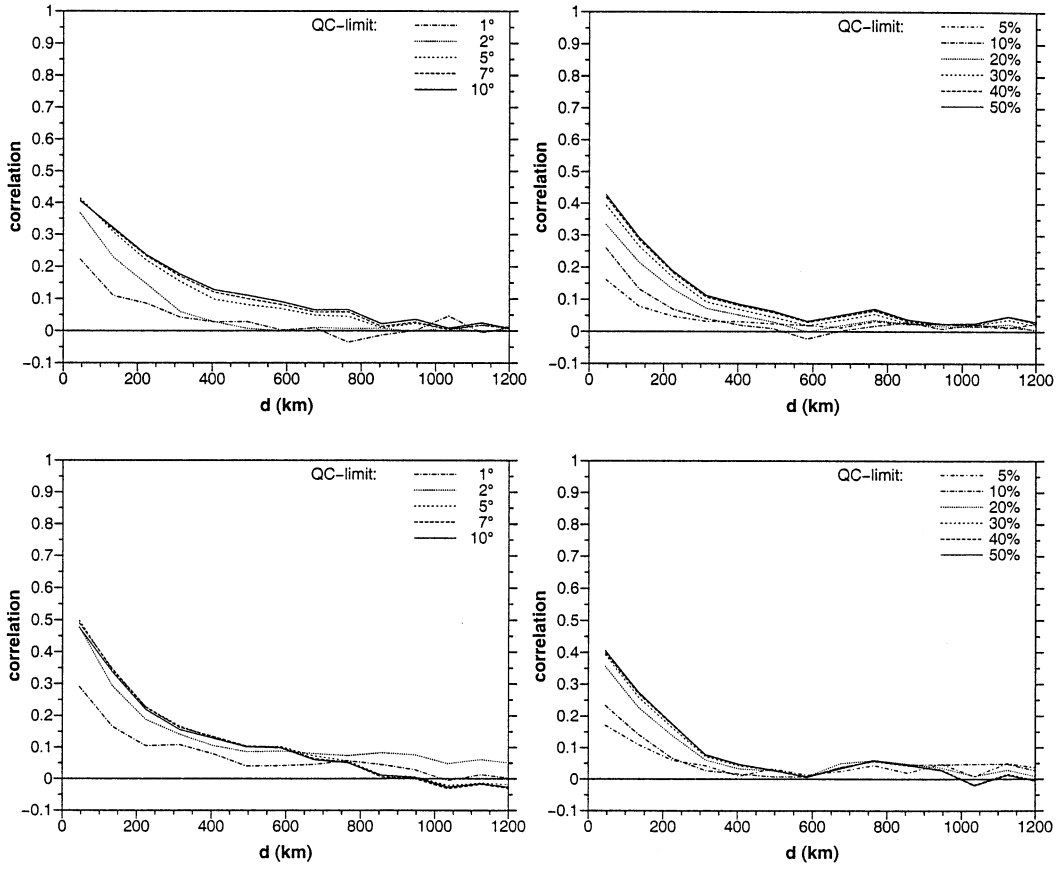

Fig. 2. Correlation of background minus observation in DMI-HIRLAM-G for T2m (left) and RH2m (right), valid for January (upper) and February (lower), respectively. The correlations are determined with six different quality control limits.

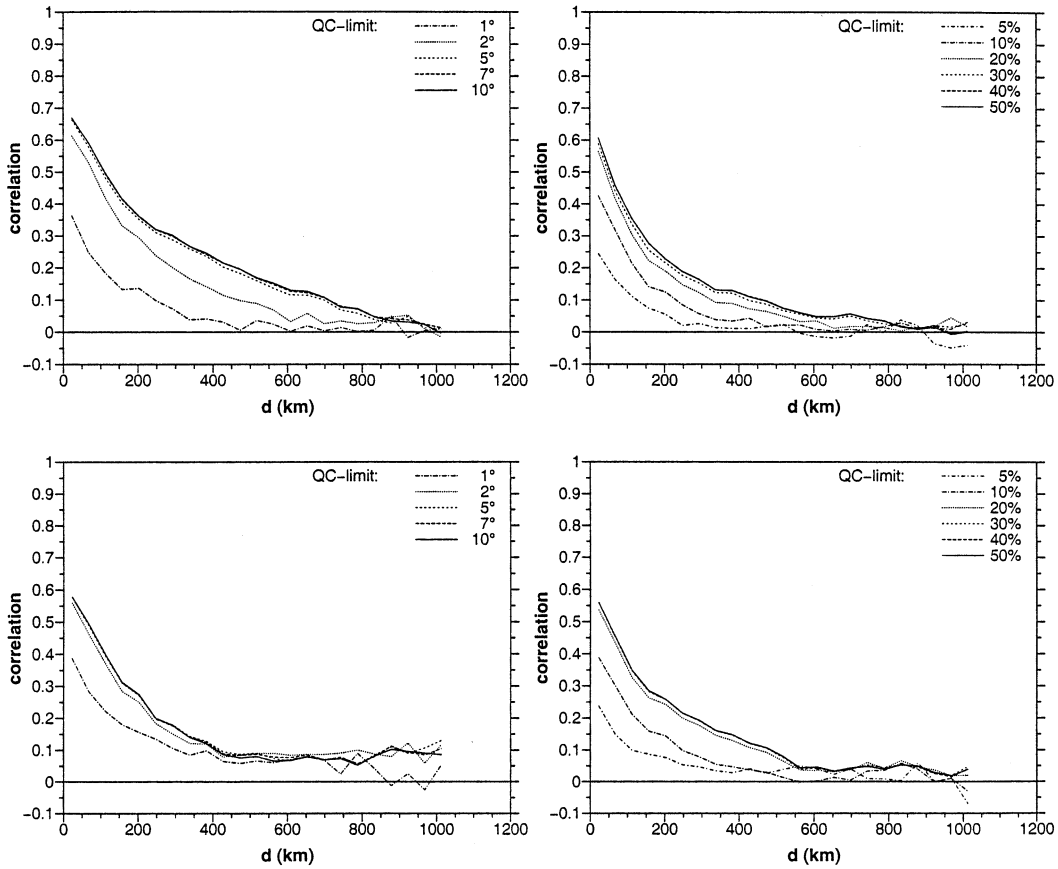

Fig. 3. Correlation of background minus observation in DMI-HIRLAM-D for T2m (left) and RH2m (right), valid for January (upper) and February (lower), respectively. The correlations are determined with six different quality control limits.

which indicates that the bias correction does not always succeed, because the bias is spatially too inhomogeneous. This is especially true for the T2m curves of the high-resolution model from February, where all curves still show some bias (Fig. 3). It is important to note that the choice of a tight quality control limit actually violates the assumption of eq. (5) that there is no correlation between observation and background errors.

It can be deduced from the curves that correlation is higher for a given distance when the quality control limit is enlarged, even though the correlations for T2m from February show a slight maximum for the 5 K and the 7 K limit (Fig. 2, lower left), also for DMI-HIRLAM-E (not shown). The reason for this may be a growing number of errors occurring above these limits, which have a random behaviour.

As a result of the above experiments, a limit of 5 K in T2m is chosen for the quality check. For RH2m, a limit of 30% seems appropriate for the further investigations.

3.3. Correlation fields

The assumption of isotropy as a major characteristic of the background error correlations is the basis for the methods described in Sections 2.1 and 2.2. The validity of this assumption is investigated here. We make use of the NMC Method in order to determine a horizontal field of the forecast error correlation for selected points within the

model domain. The data used for this investigation are taken from the operational forecasts of T2m and RH2m of DMI-HIRLAM-G and DMI-HIRLAM-D. The period is from January to June 2000.

The first location we consider is over the North Atlantic at approximately 32°W and 47°E (the upper part of Fig. 4). This point is far enough from the coast, thus avoiding possible influence from the land surface. It can be expected as a representative location for the North Atlantic area. In order to cover the surrounding area appropriately, data from DMI-HIRLAM-G are used. Both the forecast error correlation for T2m and for RH2m show a similar elliptic structure, with the major principal axes oriented SW–NE. It indicates the major flow direction, in which relatively strong advective transport of field properties, including errors, takes place. It can be expected that the influence of the predominant flow is enhanced for certain synoptic situations showing a more elliptical structure, and this may in some cases be characterized by a principal axis oriented in other directions. The assumption of isotropy in background error correlation thus seems a rather crude approximation for this location.

Another selected point is located over the North Sea (the lower part of Fig. 4). The correlation distribution is almost symmetric for this location,

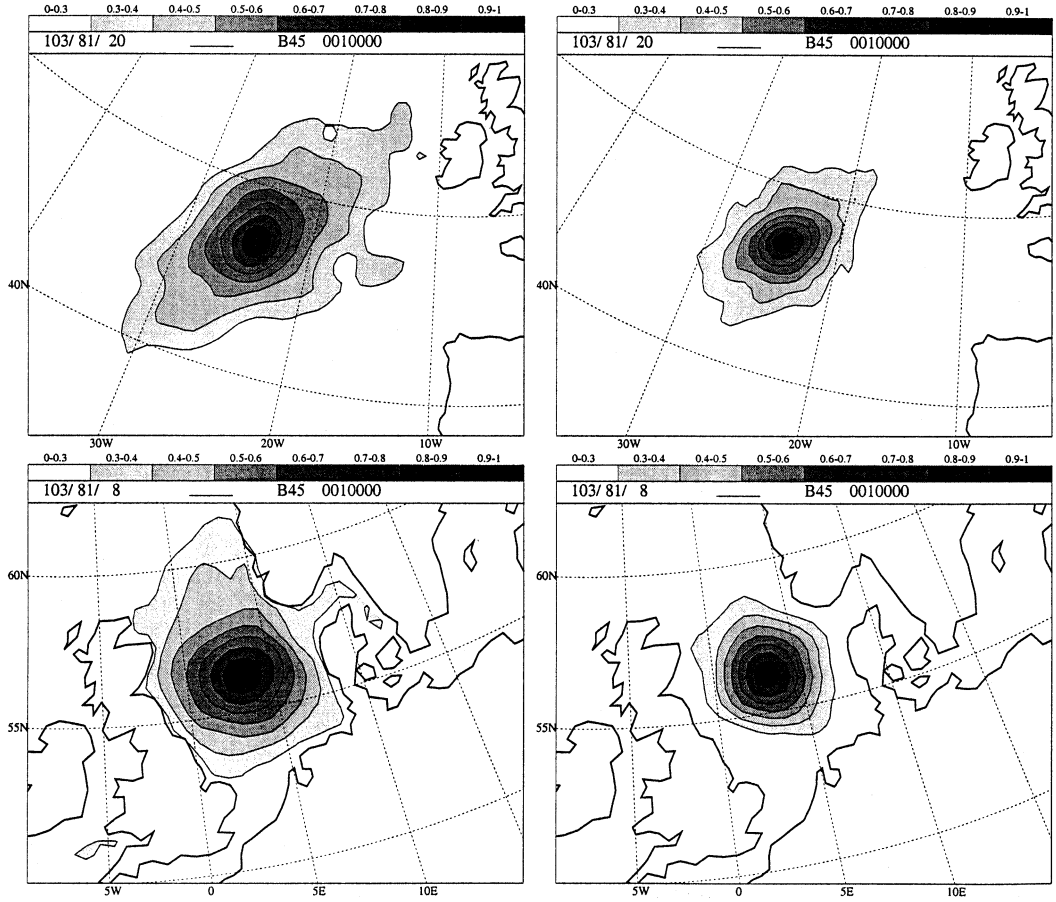

Fig. 4. Correlation fields for DMI-HIRLAM-G for T2m (left-hand frames) and RH2m (right-hand frames), determined with the NMC Method with data from the period January to June 2000. The fields are related to a point over the North Atlantic (upper frames) and to a location in the North Sea (lower frames). See text for further details.

indicating that the isotropic assumption is reasonable here. However, the influence of the land surface can be clearly recognized, at least for T2m, for which the spatial scale of correlation is large enough to reach the coastal areas.

It can be expected that model representations with grid spacings below 0.45° lead to very similar results over the sea, as other model properties remain unchanged, and grid resolution is not expected to change the isotropic properties of the background error correlations.

Figure 5 shows the correlation fields for the forecast error of T2m and RH2m in DMI-HIRLAM-D for three locations in Denmark. They represent an inland location (Bilund), a coastal point (Skagen) and an island (Lolland), respectively. The basic isotropic structure can be recognized in all three cases, although the influence of the land–sea contrast on the correlation structure is illuminating. The difference in correlation drops remarkably when the surface type changes between land and sea or vice versa.

Looking at the inland location Bilund, the correlation for T2m drops from 0.7 at the east coast of Jutland to approximately 0.45 over the sea, and is again up at 0.7 over Fyn (Fig. 5, upper left). The same behaviour occurs for RH2m, where the correlation drops from values of about 0.6 to 0.3 at Jutland east coast and shows values of almost 0.6 again over Fyn (Fig. 5, upper right).

A similar behaviour is found for the correlation field referring to Skagen, but just vice versa (Fig. 5, middle), due to the fact that the representing grid area is mainly covered by the sea. The correlation drops significantly, as soon as the Swedish and the Norwegian coast are reached. It is interesting to see in the case of T2m some correlation in forecast error between the sea (Kattegat) and the Swedish lake Vännern (Fig. 5, middle left), indicating their similar treatment within the surface model of DMI-HIRLAM-D.

The most interesting structure of forecast error correlation is shown for the island of Lolland. In both T2m and RH2m, a sharp correlation drop occurs all around the island's coast. At the northern coast, it is from 0.8 down to 0.5 for T2m (Fig. 5, lower left), and from 0.8 to 0.6 for RH2m (Fig. 5, lower right). The drop is even stronger at the southern coast, where the correlation decreases about 50% over the sea with respect to the land. As soon as the coast of Fyn, Jutland or Northern Germany is reached, the correlation becomes stronger with values over 0.6 for T2m and about 0.5 for RH2m.

The above investigations confirm that the assumption of isotropic structure functions for T2m and RH2m is just a first approximation for the background error correlations. The dependency of the structure function on the land–sea distribution is obvious and confirms the results of previous studies (Gustafsson, 1985; Häggmark et al., 2000). It can be estimated from the figures that a correlation drop of up to 50% can occur in the surface representation of DMI-HIRLAM-D. The correlation fields already indicate different horizontal scales of correlation for T2m and RH2m, where the latter is smaller than the former. This difference will be discussed in more detail in the sections below.

3.4. *Isotropic correlations*

The background error correlations are investigated for DMI-HIRLAM-G, DMI-HIRLAM-E and DMI-HIRLAM-D within this section. The dependencies on surface properties and the monthly changes of the correlations are examined. An estimation of the correlation scales is attempted.

3.4.1. Surface dependencies. As the model includes a different treatment of the surface over land and over sea, this has an influence on the background error correlations of near-surface parametres.

In order to investigate this, correlations are determined over areas with different land fraction using the NMC Method. Three classes of this kind are identified: sea, land and coastal. They are shown in Table 1 with the classification criteria. The class ranges were selected in order to separate the surface types clearly.

An additional investigation is performed by separation of points with different elevations. Five classes are identified, of which some can be considered to correspond with the classes separated with the help of the land fraction criteria (Table 1).

The correlations are calculated from operational forecast data between March and May 2000. This time interval is assumed to be large enough to be representative and to show the important differences between the different surfaces.

Looking at the results for DMI-HIRLAM-G in Fig. 6, we can deduce that for T2m the forecast

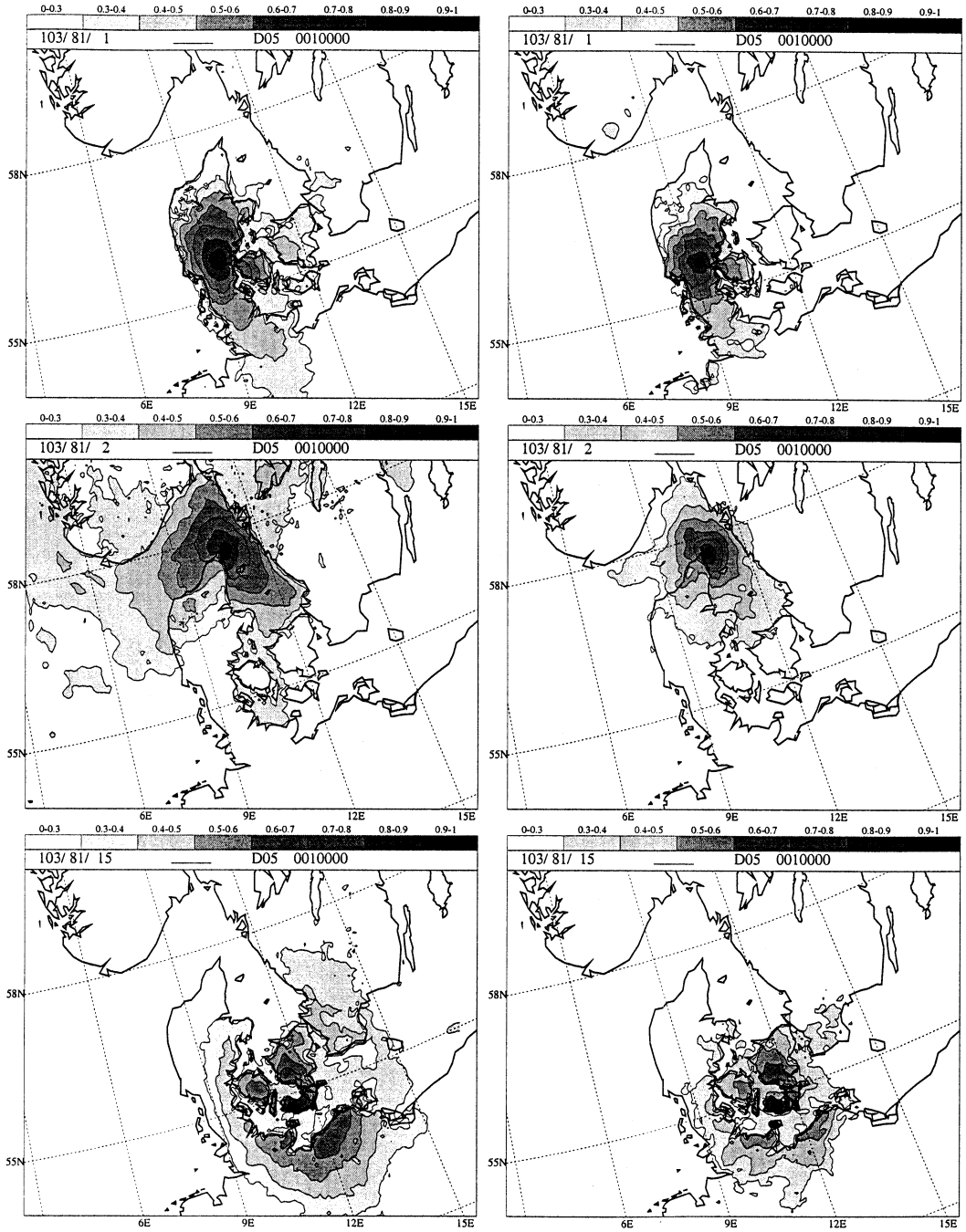

Fig. 5. Correlation fields of forecast error of DMI-HIRLAM-D, determined with the NMC Method with data from the period January to June 2000, for T2m (left-hand frames) and RH2m (right-hand frames). The upper frames show the fields relative to a point in the middle of Jutland (Bilund), the middle frames are related to a coastal point (Skagen) and the fields in the lower frames refer to an island (Lolland).

Table 1. *Classes chosen for investigating the impact of surface properties on the forecast error correlations*

Abbreviation	Criterion	Description
lfr-000	$f_l = 0$	sea
lfr-025	$5\% \leqslant f_l \leqslant 25\%$	coastal regions
lfr-100	$f_l = 100\%$	land
geo-0000	$h \leqslant 0$	sea
geo-0005	$0 < h \leqslant 0.5$ m	mainly coastal regions
geo-0100	$80\text{ m} \leqslant h \leqslant 120$ m	flat land
geo-1000	$1000\text{ m} \leqslant h \leqslant 1100$ m	hilly regions
geo-2000	$h > 2000$ m	mountainous regions

error correlations at a certain distance decrease significantly over land in comparison with sea (curves lfr-000 and lfr-100, as well as geo-0000 and geo-0100 at the left-hand side, respectively). This is also true for DMI-HIRLAM-E (Fig. 7), but the correlations from DMI-HIRLAM-D do not show this difference (Fig. 8). The situation is different for relative humidity (see right-hand side of Figs. 6–8). The correlations from DMI-HIRLAM-G show for a given distance a slight decrease over land for RH2m, but only when regarding the curves determined with the land fraction criterion. The correlations for a large distance from DMI-HIRLAM-E and DMI-HIRLAM-D, however, tend to have higher values over land for RH2m (Figs. 7 and 8, right-hand side). The figures already

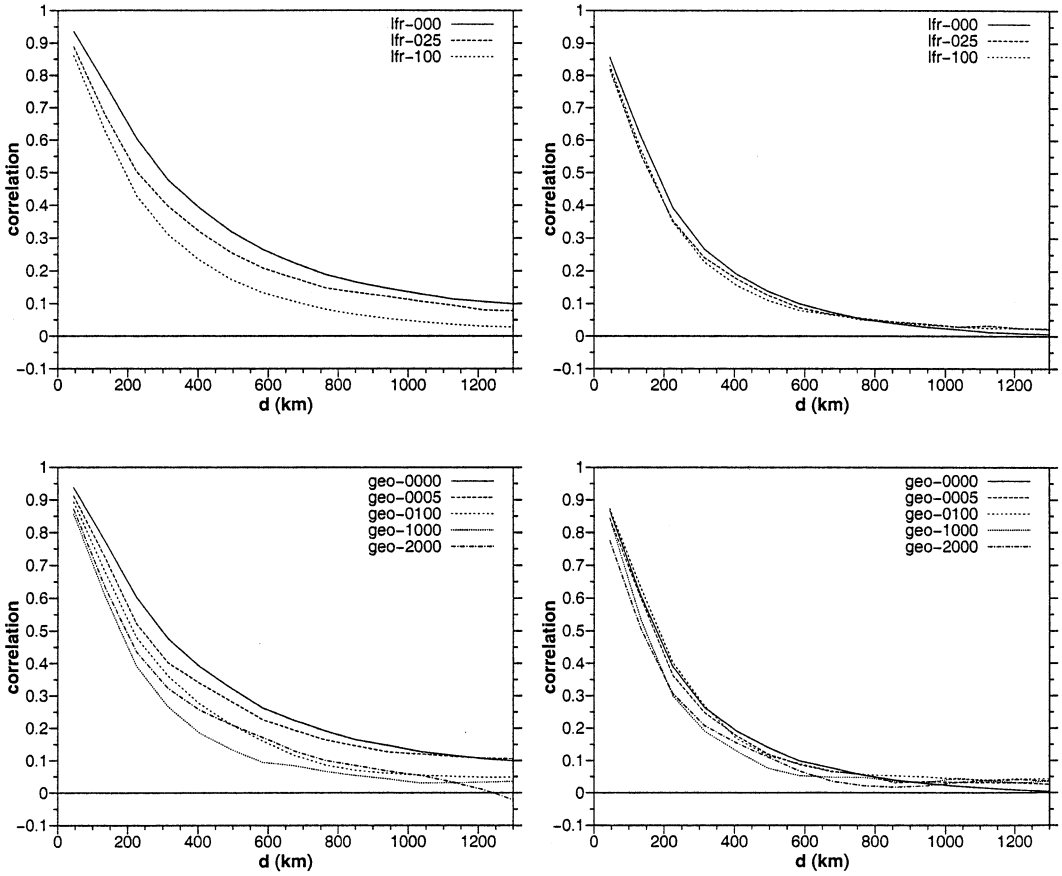

Fig. 6. Correlation in DMI-HIRLAM-G for the land fraction classes (upper) and the elevation classes (lower), as described in Table 1, valid for T2m (left) and RH2m (right). The curves are based on data from the time range 1 March to 31 May 2000.

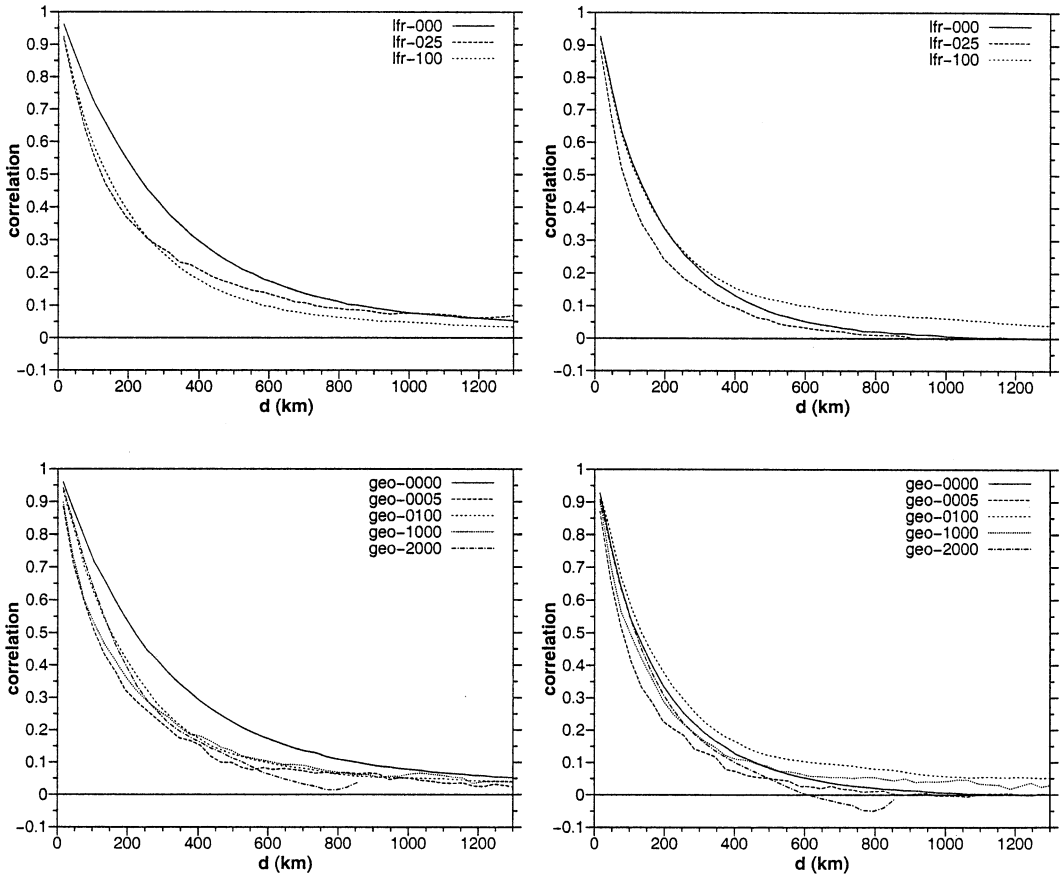

Fig. 7. Correlation in DMI-HIRLAM-E for the land fraction classes (upper) and the elevation classes (lower), as described in Table 1, valid for T2m (left) and RH2m (right). The curves are based on data from the time range 1 March to 31 May 2000.

show qualitatively a tendency towards reduced correlation scales when increasing the horizontal resolution of the model.

It is interesting to note that both the class separation by land fraction and the one for elevation reveal the same effect where the land–sea difference in correlation is concerned. The same consistency between the two class separation methods is found when comparing the correlations between coastal points (lfr-025 and geo-0005) with the other curves. Compared to the curves valid for sea (lfr-000 and geo-0000), the correlation scale decreases at the coast. This is most significant for DMI-HIRLAM-E.

A physical reason for the decrease in forecast error correlation scale of T2m near the coast and over land compared to the sea is probably that there are much more locally influenced processes due to the significant change of the surface properties than there are over sea. This is true for relative humidity only in the case of coast, and only in the correlations from the models with higher resolution.

If we consider the 2 metre temperature and compare the respective correlation curves of the land fraction classes from the three models (Figs. 6–8, upper left-hand side, respectively), we can see large variations from DMI-HIRLAM-G towards DMI-HIRLAM-D in the curve representing sea, whereas there is less difference between the curves for land. This effect also occurs in the correlation curves of the elevation classes (Figs. 6–8, lower

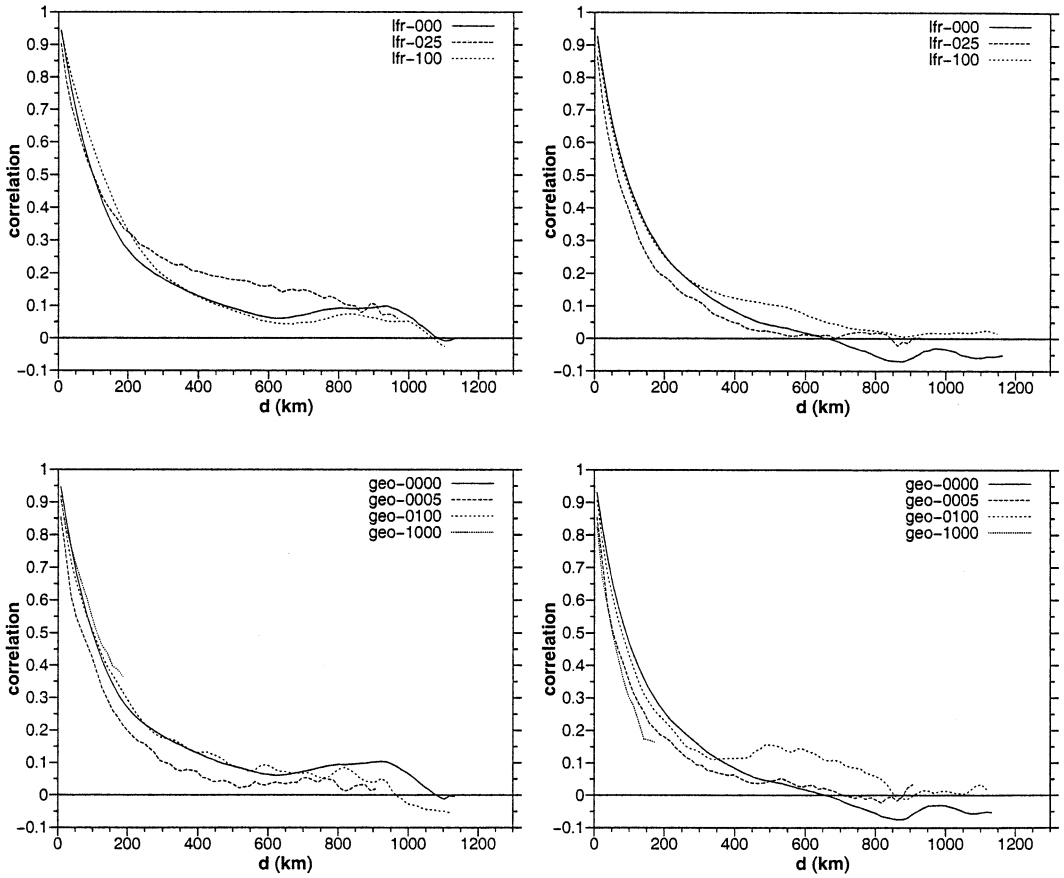

Fig. 8. Correlation in DMI-HIRLAM-D for the land fraction classes (upper) and the elevation classes (lower), as described in Table 1, valid for T2m (left) and RH2m (right). The curves are based on data from the time range 1 March to 31 May 2000.

left-hand side, respectively). It is probably due to the fact that the three models have a different coverage of the seas in their domain. In particular, DMI-HIRLAM-D covers only the North Sea and parts of the Baltic Sea, whereas DMI-HIRLAM-E and DMI-HIRLAM-G also cover the North Atlantic, where large-scale synoptic processes are dominant, in contrast to the North Sea and the Baltic Sea, which are influenced by local effects from the land.

The elevation classification includes further classes, which can be seen as representing hilly and mountainous regions (Table 1). The forecast error correlations of points from these classes are also shown in Figs. 6–8 for DMI-HIRLAM-G, DMI-HIRLAM-E and DMI-HIRLAM-D, respectively. Looking at the class for hilly regions (geo-1000), the tendency towards shorter correlation scales continues in comparison to flat land (geo-0100) and sea (geo-0000) for RH2m (lower right-hand frames in Figs. 6–8). The picture is more differentiated in T2m, where there seems to be a continued tendency towards increased correlation scale with growing elevation in DMI-HIRLAM-D, but not in DMI-HIRLAM-G (lower left-hand side frames in Figs. 6–8). There is, however, an uncertainty in these curves due to the limited number of points within the respective model domain that were found to meet the class conditions, especially for DMI-HIRLAM-D.

The class for mountainous regions (geo-2000) could only be applied to the data from DMI-

HIRLAM-G and DMI-HIRLAM-E, because DMI-HIRLAM-D does not contain enough such points. Where the forecast error correlation in relative humidity is concerned, no significant changes in the correlations with respect to hilly terrain (geo-1000) are found, but there is a tendency towards a larger correlation scale in T2m, which may reflect the special treatment of the ABL in the models.

3.4.2. Comparison and monthly changes. The forecast error for a certain atmospheric parameter depends on the uncertainties arising from the differences in the model representation for different weather situations. It is obvious that the correlation of the background error thus changes with the synoptic pattern, and the forecast quality for a certain forecast length is not constant. It is therefore of interest to see the development of the correlation curves over a series of months.

In order to make the curves determined with the Observation Method (OBM curves) and those determined with the NMC Method (NMC curves) comparable, the OBM curves are renormalized as described above (Section 2.4). This makes it possible to perform a comparison with the structure functions used in the surface analysis scheme of HIRLAM. The fitting limit d_{fit} used for the determination of the re-normalization factor in eq. (15) was chosen as 180 km for the data from DMI-HIRLAM-G. This distance is a compromise between the demand to have enough data for the fitting process and the validity of the fitting function, which is only fulfilled for small distances. The OBM curves from DMI-HIRLAM-E and DMI-HIRLAM-D were renormalized in a similar way, where d_{fit} was chosen as 60 km and 25 km, respectively.

As the observations used within the Observation Method are actually all located over land, a corresponding criteria is applied in the NMC Method in order to be consistent with the Observation Method. It should be noted that many of the observations are located in coastal regions. The criterion for grid point separation within the NMC calculations is therefore based on the land fraction and is chosen as $f_l \geqslant 5\%$.

It is possible to estimate the observation error and the background error within the Observation Method by using the covariance at zero distance [eq. (5)], which is equal to $\sigma_b^2 + \sigma_o^2$ and the fitted value for $d \to 0$, $\sigma_b^2/(\sigma_b^2 + \sigma_o^2)$ [eq. (14)]. These values are listed in Table 2, together with the estimates for σ_b and σ_o. The difference between DMI-HIRLAM-G and DMI-HIRLAM-E is rather small. Both show large estimates for the observation errors, even larger than the background error estimates. This is mainly due to the horizontal resolution of the two models, which is not consistent with the in situ observations. It is especially true for coastal stations, which make up 43% of the observations used. The exclusion of the coastal stations gives better estimates (not shown), but the statistic is less representative and the estimates are still significantly different from the estimates for DMI-HIRLAM-D. The latter appear to be much more realistic.

As the estimates for DMI-HIRLAM-D are based on a smaller sample of observations, this accounts to some extent for the large differences. An estimate for the lower resolution models using the same observation sample as for DMI-HIRLAM-D shows that about 50% of the differences in the estimates for T2m are due to the larger observation sample of DMI-HIRLAM-G and DMI-HIRLAM-E. In the case of RH2m, the portion is about 25%. A closer look at the observation samples reveals that many of the additional observations of the larger observation sample refer to medium or high elevations, which are represented rather crudely in the lower resolution models. This inconsistency in the observation representation refers to vertical displacements, and it has a stronger influence on the error estimates for T2m compared to RH2m, because vertical gradients of temperature often are stronger than those for relative humidity.

Figures 9 and 10 show the correlation curves for the first six months of the year 2000 from the three operational models at DMI, for 2 metre temperature and relative humidity, respectively. There is a clear variability from month to month in the correlations in all three models and for both parameters. Concerning T2m (Fig. 9), the variability in the OBM curves is similar for all three models, whereas the NMC curves show little less variability. The OBM curves show a general decrease in correlation scale from January to March for T2m, a high correlation in April and again lower values in May and June. The NMC curves from DMI-HIRLAM-G for T2m clearly show a trend towards smaller correlation scales

Table 2. *Estimates of the monthly observation and background standard deviations for T2m (in K) and RH2m (in %), for the models DMI-HIRLAM-G (G, grid: 0.45°), DMI-HIRLAM-E (E, grid: 0.15°) and DMI-HIRLAM-D (D, grid: 0.05°)*

		T2m				RH2m			
Model	Month	$\sigma_b^2+\sigma_o^2$	$\sigma_b^2/(\sigma_b^2+\sigma_o^2)$	σ_b	σ_o	$\sigma_b^2+\sigma_o^2$	$\sigma_b^2/(\sigma_b^2+\sigma_o^2)$	σ_b	σ_o
G	Jan	5.38	0.42	1.50	1.77	125.9	0.42	7.27	8.55
	Feb	4.89	0.51	1.58	1.55	121.4	0.42	7.14	8.39
	Mar	4.29	0.50	1.46	1.46	134.0	0.40	7.32	8.97
	Apr	5.23	0.51	1.63	1.60	128.0	0.40	7.16	8.76
	May	5.51	0.40	1.48	1.82	149.1	0.35	7.22	9.84
	Jun	4.89	0.48	1.53	1.59	142.8	0.39	7.46	9.33
E	Jan	5.38	0.45	1.56	1.72	114.9	0.46	7.27	7.88
	Feb	4.71	0.46	1.47	1.59	156.1	0.44	8.29	9.35
	Mar	4.07	0.54	1.48	1.37	131.7	0.47	7.87	8.35
	Apr	5.22	0.49	1.60	1.63	125.7	0.44	7.44	8.39
	May	5.75	0.37	1.46	1.90	156.3	0.42	8.10	9.52
	Jun	4.49	0.44	1.41	1.59	143.3	0.38	7.38	9.43
D	Jan	2.13	0.82	1.32	0.62	57.0	0.77	6.62	3.62
	Feb	1.79	0.70	1.12	0.73	46.7	0.66	5.55	3.98
	Mar	1.71	0.75	1.13	0.65	77.7	0.66	7.16	5.14
	Apr	3.01	0.73	1.48	0.90	80.1	0.69	7.43	4.98
	May	2.85	0.65	1.36	1.00	101.8	0.64	8.07	6.05
	Jun	2.15	0.72	1.24	0.78	85.1	0.71	7.77	4.97

going from January to June (Fig. 9, upper right). This tendency is also found to a lesser extent in the curves from the other models.

The OBM curves for RH2m have less variability than those for T2m and they have no obvious monthly trend. The NMC curves from DMI-HIRLAM-G for RH2m indicate the monthly trend most clearly, with decreasing correlation scales towards June, although the trend is weaker in the NMC curves of DMI-HIRLAM-E and DMI-HIRLAM-D. It should be mentioned that there is a slight inhomogeneity in the data at the end of February 2000, which is due to changes in the operational set-up of the three models. However, higher correlations at the beginning of the year can still be recognized.

The irregular behaviour of the OBM curves for large distances is connected with increased uncertainty, especially for the curves from DMI-HIRLAM-D. It should be noted that the size of the data sample is significantly smaller for the large distances and may not be sufficient to estimate the small correlations reliably. Another reason is that the points lying close to the lateral border become dominant. The latter may explain the tendency towards increasing values of the correlations from DMI-HIRLAM-D at the largest possible distances due to the treatment of the lateral boundary.

The fitted functions used for the renormalization of the OBM curves are not shown in Figs. 9 and 10, because only the fitted value for $d \to 0$ is of interest (Section 2.4). The figures include, however, the structure functions of the HIRLAM surface analysis for 2 metre temperature and relative humidity (Navascues, 1997), which are described by

$$c_r(d) = \exp\left[\sum_{n=1}^{6} a_n \left(\frac{d}{D}\right)^{n-1}\right] - 1, \qquad (17)$$

where $D = 1000$ km and the coefficients a_n as listed in Table 3 are used (NAV functions).

One difference between the application of the Observation Method and the NMC Method is that the number of points used for the correlation calculations is usually significantly higher in the latter. This is the reason for the NMC curves behaving more smoothly than the OBM curves.

As can be seen from the Figs. 9 and 10, the

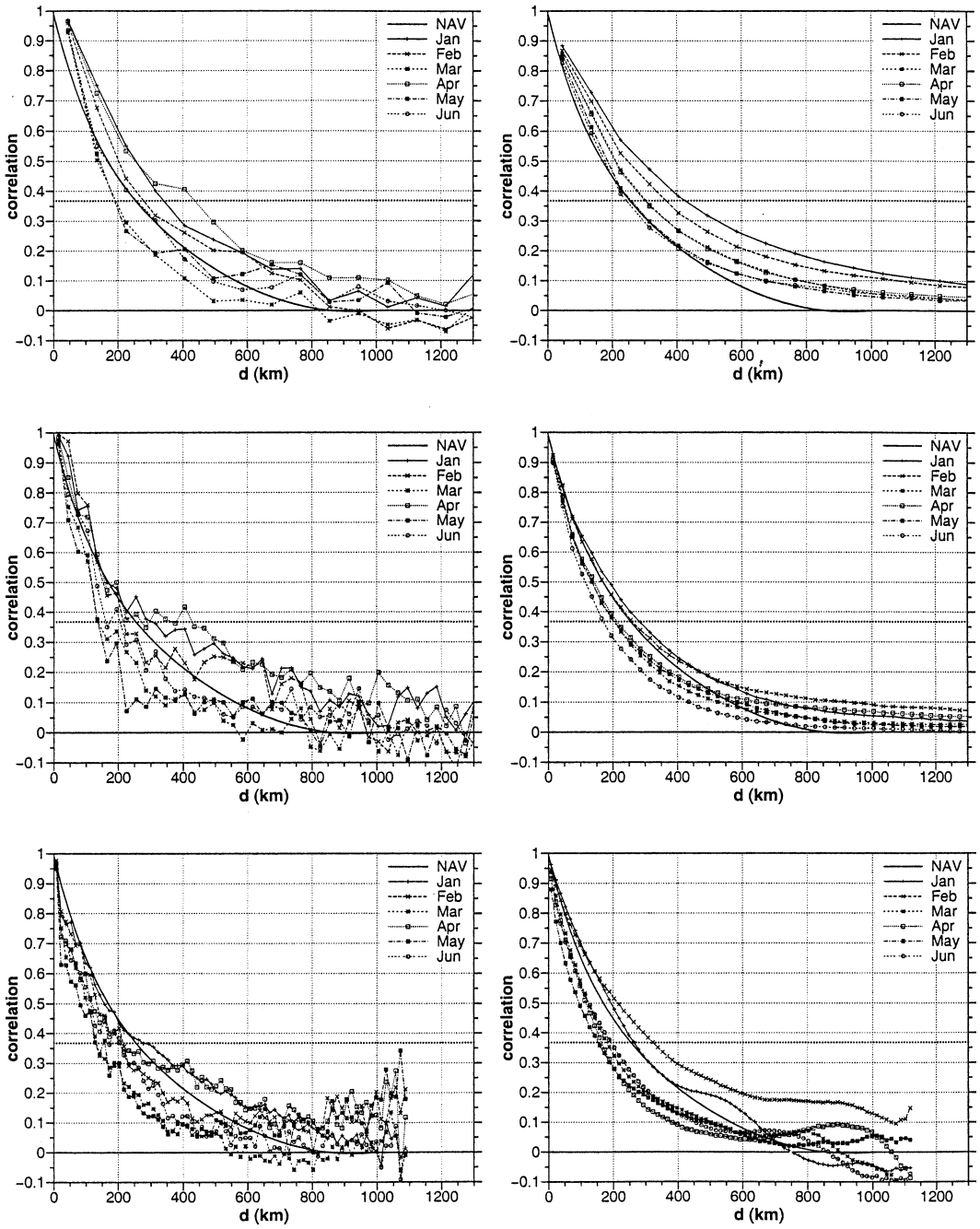

Fig. 9. Correlation curves in DMI-HIRLAM-G (upper), DMI-HIRLAM-E (middle) and DMI-HIRLAM-D (lower) for T2m, determined with the observation method (left) and the NMC Method using land points (right). Each curve represents a sample over one month. The thick solid curve (NAV) represents the function described by Navascues (1997), the horizontal dotted line depicts e^{-1}. See text for details.

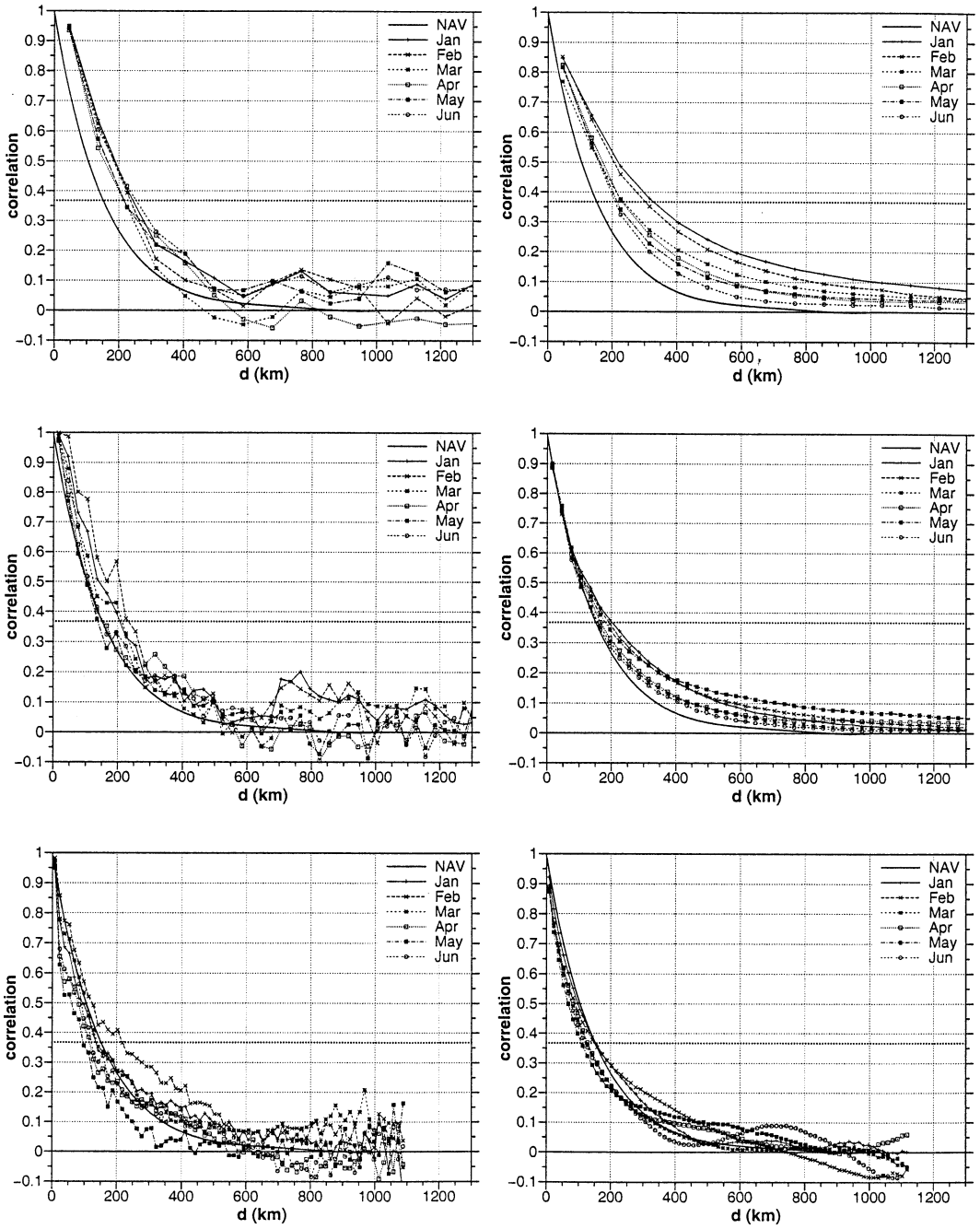

Fig. 10. Correlation curves in DMI-HIRLAM-G (upper), DMI-HIRLAM-E (middle) and DMI-HIRLAM-D (lower) for RH2m, determined with the Observation Method (left) and the NMC Method using land points (right). Each curve represents a sample over one month. The thick solid curve (NAV) represents the function described by Navascues (1997), the horizontal dotted line depicts e^{-1}. For details see text.

Table 3. *Coefficients for the structure functions of 2 meter temperature (T2m) and relative humidity (RH2m), as defined for the HIRLAM surface analysis scheme*

Parameter	a_1	a_2	a_3	a_4	a_5	a_6
T2m	0.69	−2.27	4.43	−6.43	5.11	−1.53
RH2m	0.69	−3.30	5.98	−4.37	0.47	0.53

OBM curves and the NMC curves show a tendency towards smaller correlation scales with increasing model resolution. This will be investigated quantitatively in the next subsection.

There is general correspondence between both the OBM curves and the NMC curves to the NAV functions for both T2m and RH2m. The curves from DMI-HIRLAM-G show, however, larger correlations for a certain distance than the NAV functions (Figs. 9 and 10, upper), while the curves from DMI-HIRLAM-D show lower correlation values (Figs. 9 and 10, lower). The correlations from DMI-HIRLAM-E are represented best by the NAV functions (Figs. 9 and 10, centre). It seems appropriate to re-evaluate the coefficients of the NAV functions for different models.

The NMC curves generally tend to have higher correlation values at large distances than the OBM curves do. This becomes especially clear in the curves from DMI-HIRLAM-G and DMI-HIRLAM-E (Figs. 9 and 10, upper and centre right-hand side). This effect may reflect the special character of the NMC Method that two forecast fields are correlated. Both fields are based on the model representation of the atmospheric equations and are based on the same approximations and parameterizations. A bias might still be present, and the increasing length scale with forecast period may also play a role. The correlations remain even for large distances.

3.4.3. Scale estimations. We will now try to make an estimation for the correlation distance scales by determining the distance d, where correlation reaches a value of e^{-1}. This value is chosen because the correlation curves behave like an e-function, and because the calculated curves do not descend clearly to zero at the large distances. The estimated scale is different from the differential length scale defined by the ratio between the correlation function and its Laplacian (Hollingworth and Lönnberg, 1986) by a factor of $\sqrt{2}$. It is nevertheless regarded as an appropriate distance scale to represent the correlation curves of this work.

The e^{-1} distance is estimated for each parameter, model and method by determination of an average over the months. It is summarized in Table 4. The tendency towards smaller distances with increasing model resolution is clearly pronounced for both parameters and by both methods. The correspondence of the scales between the Observation Method and the NMC Method is quite good, which indicates that the assumptions connected with the NMC Method are permissible, and that the NMC Method is an appropriate alternative to the Observation Method. A closer look at Table 4 reveals that the NMC-estimated scales are slightly larger than the corresponding OBM-estimated scales. As pointed out by Bengtsson and Gustafsson (1971), this scale may increase with forecast length. In this study, we use 36 h and 12 h forecasts to estimate forecast error with the NMC Method, while 6 h forecasts and observations are used with the Observation Method. Some corrections may be needed to account for the correlation scale growth when the NMC Method is used.

Another reason for differences between the scales from the Observation Method and the NMC Method is that the observation error σ_o is not a constant. Observations from coastal areas

Table 4. *Estimation of the distances in km, from which the correlations are dropped down to by a factor of e^{-1}. The estimations for the models are based on the respective averages over the monthly values, which are taken from the curves of Figs. 9 and 10. Further details are outlined in the text*

Method	Parameter	DMI-HIRLAM-G	DMI-HIRLAM-E	DMI-HIRLAM-D
OBM	T2m	276	204	189
	RH2m	232	182	137
NMC	T2m	316	220	203
	RH2m	250	177	131

are, for example, less representative than observations from the interior, which increases σ_o for these observations. Inclusion of such observations in the Observation Method has an influence on the re-normalization of the OBM curves (Section 2.4). It reduces the re-normalization factors and thus the scales. However, an exclusion of all coastal observations, which make up 43% of the observations used in the Observation Method, would increase the uncertainty of the statistics inappropriately.

If we compare the scales from DMI-HIRLAM-G with those from DMI-HIRLAM-D, there is a reduction of about 30% in the scale for T2m with respect to the low-resolution model, regarding the values of the Observation Method (Table 4). The reduction for RH2m is larger and approximately 40%.

The reduction is not necessarily linear to the increase in horizontal resolution. Concerning T2m, the scale for the e^{-1} value changes much more between DMI-HIRLAM-G and DMI-HIRLAM-E than it does between DMI-HIRLAM-E and DMI-HIRLAM-D. Approximate proportional behaviour of the characteristic scale with respect to horizontal resolution is found, on the other hand, for RH2m. Depending on the parameter, horizontal resolution thus is not exclusively influencing the extend to which certain meteorological scales are represented in the model. The parameterization schemes used in the model may play another important role. This will, however, not be followed up further in this work.

4. Conclusions

This study shows that the isotropy assumption of the structure functions is valid as a first approximation. Anisotropic behaviour is influenced not only by land–sea contrasts. The predominant flow has a basic influence by enlarging the correlation scale in the upstream and downstream direction, while reducing it slightly in the cross-flow direction. This dependency should be considered in the description of the structure functions in order to improve them.

The above results suggest an adaptation of the isotropic structure function for both 2 metre temperature and relative humidity when increasing the horizontal resolution of the background fields. Regarding the increase in grid spacing from 0.45 to 0.05° in DMI-HIRLAM, this adaptation should result in a reduction of the characteristic distance scale by approximately 30% in the case of 2 metre temperature, and approximately 40% in the case of 2 metre relative humidity. It is important to note that the reduction is not necessarily proportional to the increase in horizontal resolution.

The structure functions for 2 metre temperature and relative humidity depend on surface properties like land–sea contrast and elevation. There is a tendency towards smaller correlation scales over land for 2 metre temperature and along the coast for both parameters, which is due to the enhanced presence of local effects induced by strong surface contrasts. The significant drop in background error correlation in coastal areas indicates the importance of including a different treatment of such areas within a surface analysis scheme.

Estimates of the observation error and the background error for T2m and RH2m can be large in a model with a grid spacing of 0.45° or even 0.15° due to poor representation of single sites in both the horizontal (surface inhomogeneity) and in the vertical (elevation representation). The choice of the observation sample also has a significant influence on the estimates. Using an enhanced grid spacing of 0.05° as in the DMI-HIRLAM-D model for the estimates, gives, however, significantly more realistic estimates.

The results further indicate that the NMC Method is an appropriate alternative to the Observation Method in this case, which means that observation data can be avoided when determining isotropic structure functions. However, minor corrections in the derived correlation scales may be necessary. The results also suggest a decrease in the correlation scales towards summer time. Seasonal changes should be taken into account by the surface analysis in the future. Even better would be to take care of synoptic changes; however, this is more difficult and expensive to model.

5. Acknowledgments

We would like to thank Bjarne Amstrup for providing tools to extract observation data from BUFR archives. He also provided the chart for

Fig. 1. We also thank Nils Gustafsson and the reviewers for comments on the manuscript.

Appendix: List of symbols

b_{ij}^{6h}	error covariance between location i and j, referring to a 6 h forecast
Corr^{bo}	correlation of background and observation
Corr^{ff}	correlation of 12 h and 36 h forecasts
Corr^{bos}	Corr^{bo} scaled
D	correlation distance length scale
d	distance
d_{fit}	limit used for the fitting of $\mathrm{Corr}^{bo}(0)$
f_l	land fraction
$\boldsymbol{H}$	linear observation operator
h	elevation height
i, j	indices of observation locations
m, n	indices of grid point locations
r_{ij}	error covariance between point i and j
s_{ij}	sum of b_{ij}^{6h} and r_{ij}
x^{b6}	grid point value from 6 h forecast
x^{f12}, x^{f36},	forecast values from 12 h and 36 h respectively
x^t	true value, referring to a grid point
y^{b6}	value from 6 h forecast for an observation location
y^o	observed value
y^t	true value at an observation location
α	proportionality factor in the assumption of the NMC Method
Δy_{max}	quality control limit
σ_b	background error standard deviation
σ_o	observation error standard deviation

REFERENCES

Bengtsson, L. and Gustafsson, N. 1971. An experiment in the assimilation of data in dynamical analysis. *Tellus* **23**, 328–336.

Berre, L. 2000. Estimation of synoptic and mesoscale forecast error covariances in a limited-area model. *Mon. Wea. Rev.* **128**, 644–667.

Bouttier, F. 1994. A dynamical estimation of forecast error covariances in an assimilation system. *Mon. Wea. Rev.* **122**, 2376–2390.

Daley, R. 1991. *Atmospheric data analysis*. Cambridge University Press, 460 pp.

Daley, R. 1996. Generation of global multivariate error covariances by singular-value decomposition of the linear balance equation. *Mon. Wea. Rev.* **124**, 2574–2587.

Derber, J. and Buttier, F. 1999. A reformulation of the background error covariance in the ECMWF global data assimilation system. *Tellus* **51A**, 195–221.

Gandin, L. S. 1963. Objective analysis of meteorological fields. *Gidrometeorologicheskoe Izdatelstvo*, Leningrad. Translated by the Israel Program for Scientific Translations, 1965, 242 pp.

Garçia-Moya, J. A., P. del Río, Calvo, J., Navascuès, B., Esteban, L. and Calvo, M. 2000. The new operational Hirlam at INM. *Hirlam Newsletter* **35**, 59–66. Available from the Swedish Meteorological and Hydrological Institute (SMHI) Norrköping, Sweden or from the Istituto Nacional de Meteorologia (INM) Madrid, Spain.

Gustafsson, N. 1985. Development of meso-scale analysis schemes for nowcasting and very high short-range forecasting. *Proceedings from Workshop on High Resolution Analysis* ECMWF, UK, 183–212. Available from ECMWF.

Gustafsson, N., Berre, L., Hörnquist, S., Huang, X.-Y., Lindskog, M., Navascuès, B., Mogensen, K. S. and Thorsteinsson, S. 2001. Three-dimensional variational data assimilation for a limited area model. Part I: General formulation and the background error constraint. *Tellus* **53A**, 425–446.

Häggmark, L., Ivarsson, K.-I., Gollvik, S. and Olofsson, P.-O. 2000. Mesan, an operational mesoscale analysis system. *Tellus* **52A**, 2–20.

Hollingsworth, A. and Lönnberg, P. 1986. The statistical structure of short-range forecast errors as determined from radiosonde data. Part I: The wind field. *Tellus* **38A**, 111–136.

Ingleby, N. B. 2001. The statistical structure of forecast errors and its representation in the Met. Office global 3-dimensional variational data assimilation system. *Q. J. R. Meteor. Soc.* **127A**, 209–232.

Julian, P. R. and Thiebaux, H. J. 1975. On some properties of correlation functions used in optimal interpolation schemes. *Mon. Wea. Rev.* **103**, 605–616.

Källén, E. (ed.), 1996. *HIRLAM Documentation Manual system 2.5*. Available from the Swedish Meteorological and Hydrological Institute (SMHI) Norrköping, Sweden.

Lönnberg, P. and Hollingsworth, A. 1986. The statistical structure of short-range forecast errors as determined from radiosonde data. Part II: The covariance of height and wind errors. *Tellus* **38A**, 137–161.

Lorenc, A. C. 1981. A global three-dimensional multivariate statistical interpolation scheme. *Mon. Wea. Rev.* **109**, 701–721.

Lorenc, A. C. 1986. Analysis methods for numerical weather prediction. *Q. J. R. Meteor. Soc.* **112**, 1177–1194.

Lorenc, A. C., Ballard, S. P., Bell, R. S., Ingleby, N. B., Andrews, P. L. F., Barker, D. M., Bray, J. R., Clayton, A. M., Dalby, T., Li, D., Payne, T. J. and Saunders, F. W. 2000. The Met. Office global three-dimensional variational data assimilation scheme. *Q. J. R. Meteor. Soc.* **126**, Part B, 2991–3012.

Navascuès, B. 1997. *Analysis of 2 meter temperature and relative humidity*. Hirlam Tech. Rep., 28. Available from the Swedish Meteorological and Hydrological Institute (SMHI) Norrköping, Sweden or from the Istituto Nacional de Meteorologia (INM) Madrid, Spain.

Parrish, D. F. and Derber, J. C. 1992. The National Meteorological Centre's statistical interpolation analysis system. *Mon. Wea. Rev.* **120**, 1747–1763.

Puri, K. and Lönnberg, P. 1991. Use of high-resolution structure functions and modified quality control in the analysis of tropical cyclones. *Mon. Wea. Rev.* **119**, 1151–1167.

Rabier, F., McNally, A., Andersson, E., Courtier, P., Eyre, J., Hollingsworth, A. and Bouttier, F. 1998. The ECMWF implementation of three dimensional variational assimilation (3D-Var). Part II: Structure functions. *Q. J. R. Meteor. Soc.* **124**, 1809–1830.

Rutherford, I. D. 1972. Data assimilation by statistical interpolation of forecast error fields. *J. Atmos. Sci.* **29**, 809–815.

Sass, B. H., Nielsen, N. W., Jørgensen, J. U. and Amstrup, B. 1999. *The operational HIRLAM system at DMI — October 1999*. Tech. Rep., 99-21. Available from the Danish Meteorological Institute (DMI) Copenhagen, Denmark.

Sattler, K., Amstrup, B., Hilden, A. and Hansen, J. 2000. *Evaluation of the HIRLAM surface analysis scheme for 2 meter temperature and relative humidity by comparison with AMIS gridded observations*. Tech. Rep., 00-09. Available from the Danish Meteorological Institute (DMI) Copenhagen, Denmark.